Elastic behavior of MFI-type zeolites:Compressibility of H-ZSM-5 in penetrating and non-penetrating media

Journal of Solid State Chemistry 184 (2011) 1505–1516

Contents lists available at ScienceDirect

Journal of Solid State Chemistry

journal homepage: www.elsevier.com/locate/jssc

Elastic behavior of MFI-type zeolites: Compressibility of H-ZSM-5 in penetrating and non-penetrating media

Simona Quartieri [a,*], Gabriele Montagna [b], Rossella Arletti [c], Giovanna Vezzalini [b]

[a] Dipartimento di Scienze della Terra, Università di Messina, Viale Ferdinando Stagno d'Alcontres 31, 98166 Messina S. Agata, Italy
[b] Dipartimento di Scienze della Terra, Università di Modena e Reggio Emilia, Via S. Eufemia 19, 41100 Modena, Italy
[c] Dipartimento di Scienze Mineralogiche e Petrologiche, Via Valperga Caluso 35, 10125 Torino, Italy

ARTICLE INFO

Article history:
Received 21 December 2010
Received in revised form
7 April 2011
Accepted 10 April 2011
Available online 20 April 2011

Keywords:
MFI zeolite
H-ZSM-5
High pressure structure
Elastic behavior
Synchrotron X-ray powder diffraction

ABSTRACT

The elastic behavior of H-ZSM-5 was investigated by in-situ synchrotron X-ray powder diffraction, using both silicone oil (s.o.) and (16:3:1) methanol:ethanol:water (m.e.w.) as "non-penetrating" and "penetrating" pressure transmitting media, respectively. From P_{amb} to 6.2 GPa the volume reduction observed in s.o. is 16.6%. This testifies that H-ZSM-5 is one of the most flexible microporous materials up to now compressed in s.o. Volume reduction observed in m.e.w. up to 7.6 GPa is 14.6%. A strong increase in the total electron number of the extraframework system, due to the penetration of water/alcohol molecules in the pores, is observed in m.e.w. This effect is the largest up to now observed in zeolites undergoing this phenomenon without cell volume expansion. The higher compressibility in s.o. than in m.e.w. can be ascribed to the penetration of the extra-water/alcohol molecules, which stiffen the structure and contrast the channel deformations.

1. Introduction

Zeolites with MFI topology [1] are of great interest due to their wide impact as shape-selective industrial catalysts with tunable acid strength. Their unique structure consists of intersecting channels formed by 10 $(Al,Si)O_4$ tetrahedra [2,3] with a diameter of 5–6 Å, which enables compounds of comparable size to enter and diffuse into the channels (Fig. 1).

In general, MFI-type porous materials show a high flexibility of the framework depending on temperature, Si/Al ratio and extraframework content [4,5]. In particular, a reversible temperature-induced phase transition from monoclinic ($P2_1/n$) to orthorhombic (*Pnma*) space group (s.g.) is observed as the result of the relative shift of (0 1 0) pentasil layers in the *c* direction [6]. In all-silica MFI phases, the transition occurs at about 320 K, while the introduction of aluminum lowers this temperature. For SiO_2:$Al_2O_3 < 110$ (> 0.8% wt Al), the transition temperature is below room temperature [4], hence the s.g. is *Pnma*. As the flexibility of the framework can play a role in the processes involved in the catalysis, like diffusion and adsorption, it is our aim to understand how this flexibility is influenced by another thermodynamic variable, *i.e.* pressure.

For these reasons, as part of a wider project aimed to the study of the elastic behavior of microporous materials [7–15], we have performed in-situ synchrotron X-ray powder diffraction (XRPD) experiments on MFI-type zeolites with different framework Si/Al ratio and different extraframework content – namely Na-ZSM-5 [16], H-ZSM-5, and silicalite and mutinaite [17,18] – using (16:3:1) methanol:ethanol:water (m.e.w.) and/or silicone oil (s.o.) as pressure-transmitting media. The former medium, and in general the aqueous ones, have been demonstrated to be able to penetrate the zeolite pores [12,15–19], and so have been defined "penetrating" P-transmitting media. On the contrary, s.o. is constituted by too large molecules to penetrate the channels, hence is a "non-penetrating" medium [7–11,13,14].

In a very recent paper [16] we have reported the results of our study on the elastic behavior of Na-ZSM-5. The complete structural refinements performed on this phase compressed in m.e.w. up to 1.6 GPa, revealed a strong increase in the extra-framework content—with the penetration of additional water/alcohols molecules of the medium in the partially occupied extraframework sites of as-synthesized Na-ZSM-5. This P-induced penetration, which does not induce any cell volume expansion, is only partially reversible, since a fraction of the extra-molecules remain in the channels upon decompression. Concerning the results obtained in s.o., Na-ZSM-5 resulted to be the most compressible microporous material among those so far studied with "non-penetrating" media. Moreover, its compressibility is higher in s.o. than in m.e.w. ($K_0 = 18.2(6)$ GPa, $K' = 4$ (fixed) and 28.9(5) GPa, $K' = 4$ (fixed)), due to the fact that the penetration of the extra-water/alcohol molecules contributes to stiffen the structure and contrasts the P-induced channels deformations.

In the present paper we discuss the high-pressure (HP) behavior of H-ZSM-5, another synthetic phase with MFI topology. In particular, the specific aims of the work are: (i) to investigate

* Corresponding author.
E-mail address: squartieri@unime.it (S. Quartieri).

0022-4596/$ - see front matter © 2011 Elsevier Inc. All rights reserved.
doi:10.1016/j.jssc.2011.04.026

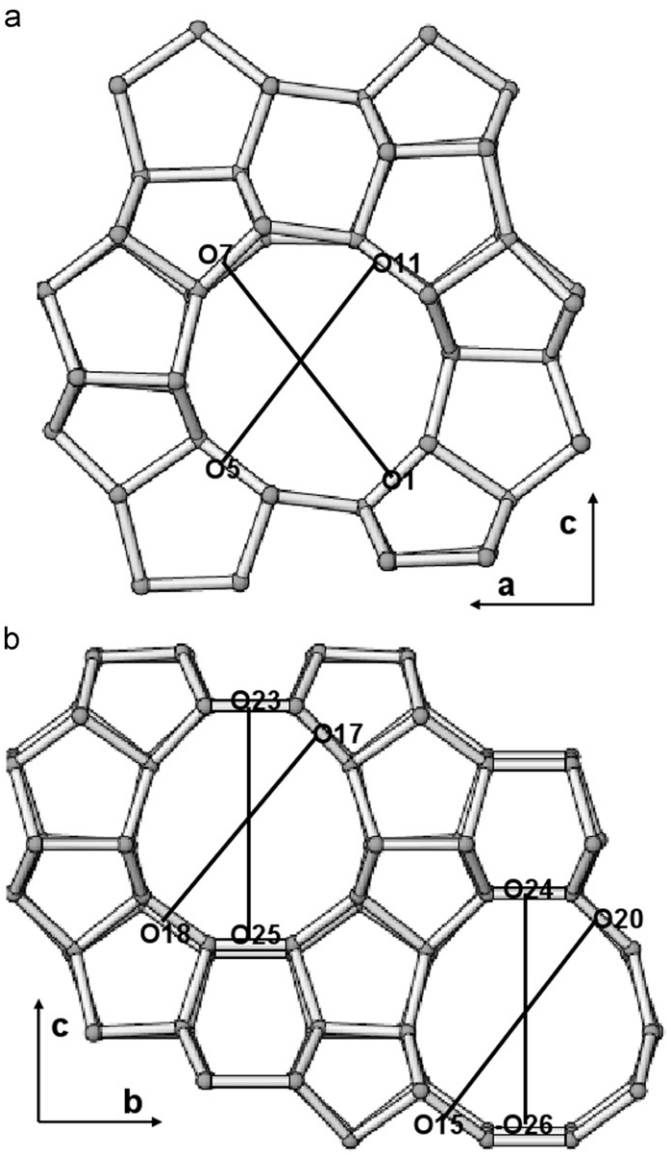

Fig. 1. (a) Projection of H-ZSM-5 structure along [0 1 0], showing the straight channels running parallel to the *b* axis; (b) (1 0 0) layer, showing the apertures of the sinusoidal channels running along *a* axis. The labeled atoms are used to measure the channel diameters (see text and Fig. 7).

the stability, the elastic behavior and the HP-structural evolution of H-ZSM-5 by means of in-situ synchrotron XRPD, using both "penetrating" and "non-penetrating" P-transmitting media; (ii) to verify the capacity of this phase to host additional molecules inside its structure; (iii) to single out the reversibility degree of the HP-induced structural modifications; and (iv) to compare H-ZSM-5 HP structural evolution with that of Na-ZSM-5, so to investigate the effect of the different framework and extraframework composition on the response to compression of these two microporous materials with the same topology.

2. Experimental methods and data analysis

2.1. Chemical analysis

The composition of the H-ZSM-5 sample was determined by electron microprobe analysis, carried out using an ARL-SEMQ instrument in wavelength dispersive mode, operating at 15 kV and with a beam current of 20 nA and diameter of 30 μm; counting times of 5, 10, and 5 s on high background, peak, and low background, respectively, were used. A pellet of 10 mg of powdered H-ZSM-5 sample was prepared by applying a pressure of 10 ton m^{-2}. The standards used were albite Amelia for Si and Na, microcline AB for K and Al, paracelsiane for Ba, anorthite for Sr, synthetic anorthite 70% for Ca, and olivine P140 for Mg, and Fe. The data acquisition and processing were performed using the PROBE program [20]. Water content was determined by thermogravimetric analysis on a 10 mg sample using a Seiko SSC/5200 instrument, operating at 10 °C/min from 18 to 1000 °C in air. The weight loss was 10.0%. The chemical formula calculated on the basis of 192 oxygen atoms and on the average of four point analyses is: $[(H_{6.8}\ Na_{1.1})\ (Al_{7.9}\ Si_{89.8})\ O_{192}\ 36\ H_2O$; s.g. *Pnma*], Si/Al=11.4.

2.2. HP X-ray powder diffraction experiments

The HP synchrotron XRPD experiments were performed at ID09 and at SNBL1 (BM01a) beamlines of ESRF, using a modified Merrill-Bassett DAC [21], and both s.o. and m.e.w. as P-transmitting media. Table 1 reports selected experimental parameters relative to the two types of experiments. Pressure was calibrated using the ruby fluorescence method [22] on the non-linear hydrostatic pressure scale [23]. The estimated precision in the pressure values is 0.1 GPa. The experiments in s.o. were performed from P_{amb} to 8.0 GPa, while those in m.e.w. from P_{amb} to 7.6 GPa. Some other patterns were collected upon decompression, from the highest pressure to P_{amb} [labeled (rev) in the following]. One-dimensional diffraction patterns were obtained by integrating the two dimensional images with the program FIT2D [24]. Selected integrated patterns are shown in Fig. 2a and b, for s.o. and m.e.w., respectively.

Unit cell parameters were determined by Rietveld profile fittings – using GSAS package [25] with the EXPGUI [26] interface – up to 6.2 GPa in s.o. (being the data quality of the higher pressure patterns too low for the refinement), and up to 7.6 GPa in m.e.w. The background curves were fitted by a Chebyshev polynomial. The pseudo-Voigt profile function proposed by Thomson et al. [27] and cut-off of the peak intensity were applied. The refined cell parameters as a function of pressure are reported in Table 2 and Figs. 3 and 4 (a and b) for s.o. and m.e.w., respectively.

The quality of the powder data collected in m.e.w. allowed to perform complete structural refinements up to 2.0 GPa (see Fig. 2c).

Table 1
Experimental and structural refinement parameters for the XRPD measurements in silicone oil (s.o.) and (16:3:1) methanol:ethanol:water (m.e.w.).

	Experiments in s.o. (ID09 beamline, ESRF)	**Experiments in m.e.w. and at ambient conditions (BM01A beamline, ESRF)**
λ	0.4132	0.70026
Detector	MAR345 (pixel dimension=150 μm)	MAR345 (pixel dimension=150 μm)
Sample-detector distance (mm)	365	221
Beam size (μm)	60	100
Exposure time (s)	30	180
P-range (GPa)	P_{amb}–8.0	P_{amb}–7.6
Δ*P* increment (GPa)	0.2–0.7	0.2–0.7
Sample equilibration time (min)	15	30
Integration 2θ range of the powder patterns (deg)	1.3–26	2–38
No. of coefficients used in the Chebyshev polynomial	18	18

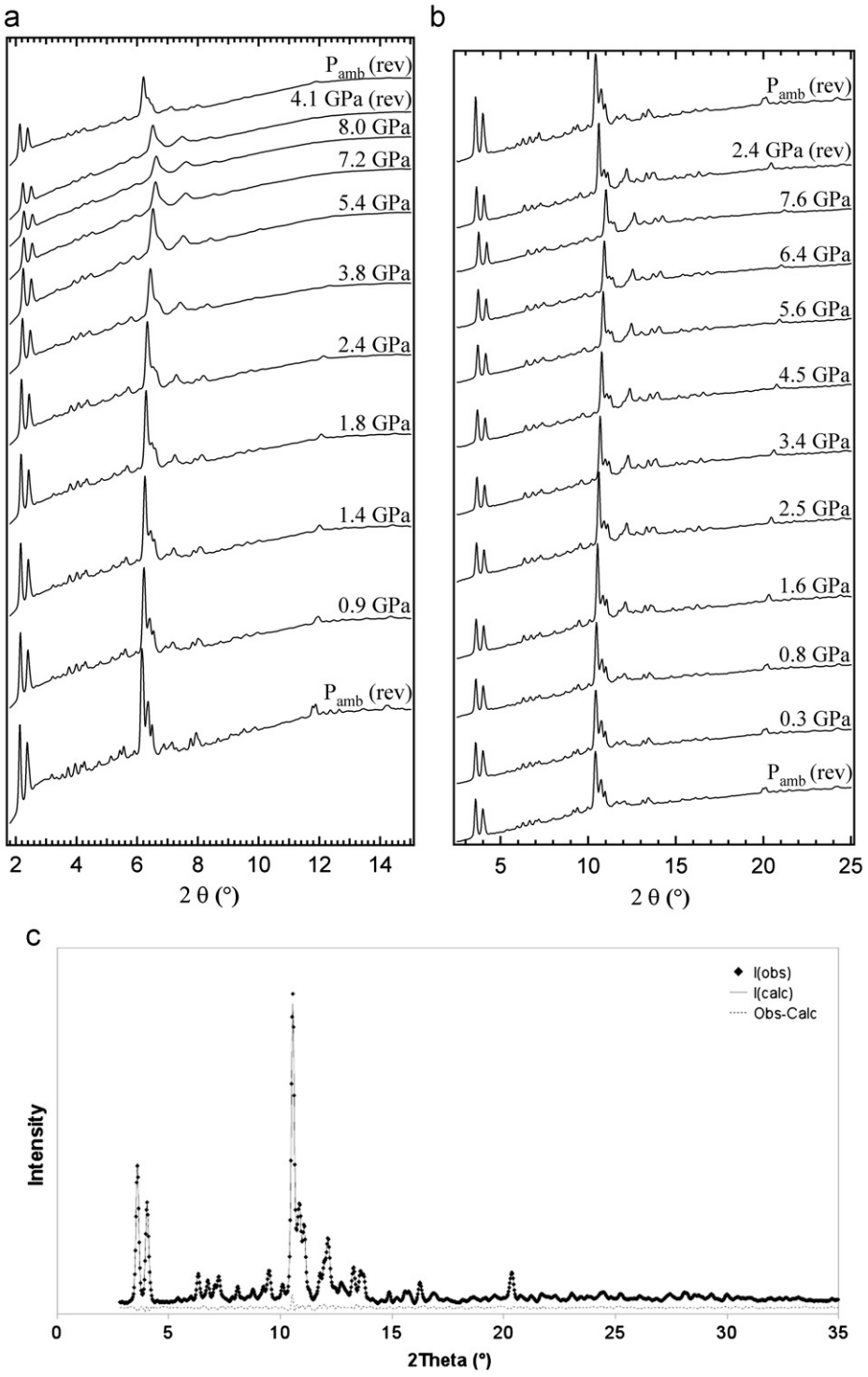

Fig. 2. Selected integrated powder patterns, collected in silicone oil (a), and (16:3:1) methanol:ethanol: water (b), reported as a function of pressure. The patterns at the top of the figures were collected during decompression. (c) Observed (crossed) and calculated (continuous line) diffraction patterns and the final difference curve from Rietveld refinement of H-ZSM-5 compressed in m.e.w. at 2 GPa.

Consistently with the chemical composition, in particular with the Si/Al ratio of 11.4, the symmetry is *Pnma*. The structures of both mutinaite [28] and a H-ZSM-5 sample from literature [29] were used as starting models for the refinement at P_{amb}, since they gave the lowest $R/F^{**}2$ value in the first cycle of the refinement. The two models provided comparable results; those reported in the following were obtained starting from mutinaite structure. The following refinement strategy was used for all the structural refinements: (i) the zero-shift and the unit cell parameters were allowed to vary in alternated cycles at the first stages of the refinement, while the scale factor remains almost constant for all the pattern refinements; (ii) after the initial refinement cycles, the refined structural parameters for each data histogram were: fractional coordinates for all atoms (soft-restraints were applied to the T–O distances [Si–O=1.58(2)–1.63(2)] and the weight was gradually decreased after the initial stages of refinement, up to a final weight equal to 10), occupancy factors for extraframework sites and thermal isotropic displacement factors for all atoms (the isotropic displacement

Table 2
Unit-cell parameters of H-ZSM-5 at the investigated pressures, using silicone oil (s.o.) and (16:3:1) methanol:ethanol:water (m.e.w.).

P (GPa)	a (Å)	b (Å)	c (Å)	V (Å^3)
s.o.				
P_{amb}	20.189(1)	19.995(2)	13.460(1)	5433(1)
0.2	20.141(1)	19.956(1)	13.431(1)	5399(1)
0.9	19.973(2)	19.846(2)	13.347(2)	5291(1)
1.1	19.913(2)	19.818(3)	13.317(2)	5255(1)
1.4	19.839(3)	19.788(4)	13.281(2)	5214(1)
1.6	19.759(4)	19.764(5)	13.244(3)	5172(2)
1.8	19.681(4)	19.726(5)	13.204(2)	5126(2)
2.1	19.599(4)	19.678(4)	13.160(3)	5075(2)
2.4	19.512(4)	19.642(5)	13.121(4)	5029(2)
2.7	19.440(4)	19.560(5)	13.069(4)	4970(3)
3.0	19.357(5)	19.510(5)	13.031(5)	4921(2)
3.3	19.292(5)	19.439(5)	12.986(4)	4870(3)
3.8	19.199(5)	19.358(6)	12.933(5)	4807(3)
4.2	19.135(5)	19.302(6)	12.898(5)	4764(3)
4.6	19.066(6)	19.241(6)	12.850(6)	4717(4)
5.0	19.003(6)	19.185(7)	12.825(6)	4676(4)
5.4	18.949(7)	19.134(7)	12.802(7)	4641(5)
5.8	18.892(7)	19.085(7)	12.773(7)	4606(4)
6.2	18.833(7)	19.033(8)	12.749(7)	4570(5)
4.1 (rev)	18.957(7)	19.163(7)	12.891(7)	4683(5)
P_{amb} (rev)	19.933(4)	19.988(5)	13.466(3)	5365(2)
m.e.w.				
P_{amb}	20.174(2)	19.995(2)	13.458(1)	5429(1)
0.1	20.164(2)	19.986(2)	13.453(1)	5422(1)
0.3	20.142(2)	19.967(2)	13.443(1)	5407(1)
0.5	20.103(2)	19.942(2)	13.427(1)	5383(1)
0.8	20.044(2)	19.913(2)	13.407(1)	5351(1)
1.2	19.958(2)	19.869(2)	13.381(1)	5306(1)
1.6	19.899(2)	19.823(2)	13.360(1)	5270(1)
2.0	19.828(2)	19.764(2)	13.331(1)	5224(1)
2.5	19.754(3)	19.697(3)	13.290(2)	5171(1)
3.0	19.670(3)	19.629(3)	13.250(2)	5116(1)
3.4	19.597(3)	19.556(3)	13.209(2)	5062(1)
4.1	19.473(5)	19.449(4)	13.142(3)	4977(2)
4.5	19.413(4)	19.406(4)	13.116(2)	4941(2)
5.0	19.339(5)	19.347(4)	13.073(3)	4891(2)
5.6	19.234(5)	19.278(4)	13.024(3)	4829(2)
6.2	19.136(5)	19.208(5)	12.977(3)	4770(2)
6.4	19.098(5)	19.192(5)	12.962(3)	4751(2)
6.9	19.007(5)	19.108(5)	12.906(3)	4687(2)
7.6	18.926(5)	19.039(5)	12.861(3)	4634(2)
4.9	19.291(6)	19.327(5)	13.051(3)	4866(2)
2.4	19.755(3)	19.705(3)	13.293(2)	5175(2)
P_{amb} (rev)	20.164(2)	19.981(2)	13.451(2)	5419(2)

parameters were constrained in the following way: the same value for all tetrahedral cations, a second value for all framework O atoms, and a third one for all the extra-framework sites); and (iii) occupancy factors and isotropic thermal displacement parameters for extraframework sites were varied in alternate cycles. All the extraframework sites were refined with the oxygen scattering curve, as discussed below.

Table 3 reports the details of the four selected structural refinements at P_{amb}, 0.8, 2.0 GPa and P_{amb} (rev) which will be discussed in the following.

The isothermal bulk moduli of H-ZSM-5 compressed in s.o. and m.e.w. were determined with the EOS-FIT program [30], using a truncated second-order Birch–Murnaghan equation of state [31]. The elastic behavior along the axes was described with a "linearized" Murnaghan equation of state [32].

3. Results and discussion

Fig. 2a and b – reporting selected powder patterns of H-ZSM-5 collected in s.o. and m.e.w., respectively – shows that the decrease of the peak intensities with the increasing pressure is more evident in the patterns collected with the "non-penetrating" P-transmitting medium. Moreover, these patterns show a larger broadening of the peak profiles. In addition, while the intensities and positions of the diffraction peaks are reversibly regained upon decompression in m.e.w. experiment, the reversibility is only partial in s.o. one.

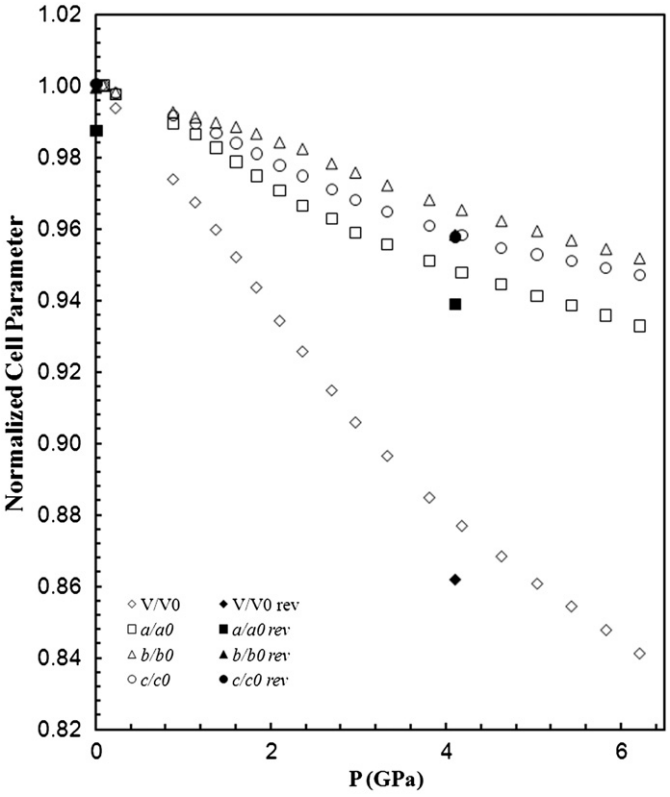

Fig. 3. Variation of H-ZSM-5 lattice parameters as a function of pressure measured in silicone oil (s.o.). The errors associated with the cell parameters are smaller than the symbol size.

Even if H-ZSM-5 was compressed in s.o. up to 8.0 GPa, the unit cell parameters were successfully refined only up to 6.2 GPa. In this P-range, the reductions of a, b, c, and V are: 5.9%, 6.0%, 5.7% and 16.6%, respectively (Table 2 and Fig. 3). The unit cell parameters corresponding to ambient conditions are only partially recovered upon pressure release; in particular, a large hysteresis effect is observed for the a axis and, consequently, for the cell volume, which remain, upon decompression, smaller than those of the starting H-ZSM-5.

Concerning the results obtained compressing H-ZSM-5 in m.e.w., a unit cell volume reduction of 14.6% is observed between P_{amb} and 7.6 GPa, while the unit cell axes undergo the following contractions: $\Delta a = 5.8\%$, $\Delta b = 4.8\%$, $\Delta c = 4.4\%$ (Table 2 and Fig. 4a,b). An almost isotropic behavior of the unit cell axes is observed up to about 0.5 GPa (Fig. 4b), while above this pressure an increasing anisotropy characterizes the response to compression of the cell parameters. Figs. 2b, 4a,b and Table 2 show that the HP-induced modifications of the cell parameters of H-ZSM-5 in m.e.w. are reversible upon pressure release up to ambient conditions.

3.1. HP-induced structural deformations and medium penetration of H-ZSM-5 compressed in m.e.w.

The structural response of H-ZSM-5 to compression in m.e.w. was followed by means of 9 complete Rietveld structural refinements, performed from P_{amb} to 2.0 GPa and at P_{amb} (rev). Above 2 GPa, the pattern quality and the high number of the structural

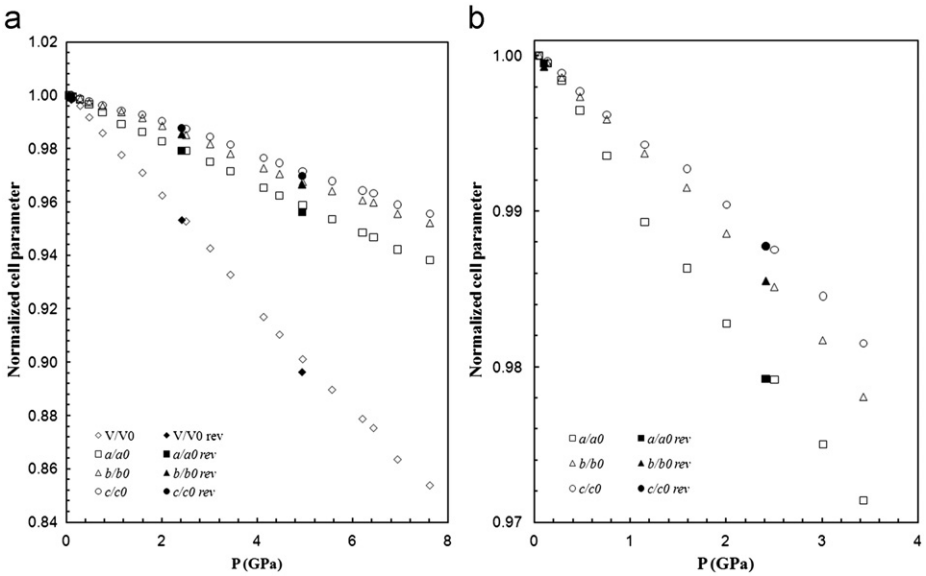

Fig. 4. (a) Variation of H-ZSM-5 lattice parameters as a function of pressure measured in (16:3:1) methanol:ethanol:water (m.e.w). (b) detail of the *P* range between P_{amb} and 4 GPa. The errors associated with the cell parameters are smaller than the symbol size.

Table 3
Details of the four selected structural refinements of H-ZSM-5 at P_{amb}, 0.8, 2.0 GPa and P_{amb} (rev).

	P_{amb}	0.8 GPa	2.0 GPa	P_{amb} (rev)
R_p	0.036	0.036	0.030	0.039
Rw_p	0.047	0.046	0.040	0.054
$R_{F^{**}2}$	0.061	0.064	0.047	0.054
No. of variables	134	134	134	134
No. of observations	1984	1962	1914	1982

parameters did not allow reliable structural data to be obtained. The atomic coordinates refined at four selected pressure values (P_{amb}, 0.8, 2.0 GPa and P_{amb} (rev)) are reported in Table 4. Tables 5 and 6 report the framework and extra-framework bond distances, respectively.

3.1.1. Framework

The structural variations induced on the framework up to 0.8 GPa are rather small, consistently with the small decrease of the unit cell parameters in this P-range ($\Delta a = 0.6\%$, $\Delta b = 0.4\%$, $\Delta c = 0.4\%$, and $\Delta V = 1.4\%$). Above this pressure, the 10-ring surrounding the channel along [0 1 0] becomes more elliptic (Fig. 5), while those surrounding the channels along [1 0 0] remain rather circular (Fig. 6). These observations can be quantitative discussed on the basis of Table 7 and Fig. 7, which report the diagonal O…O distances and the ellipticity of both channels against pressure. The channel ellipticity [33] is defined as the ratio between the longest and shortest pore dimensions [O1–O7 and O5–O11 distances for the straight channels (Fig. 1), and O15–O20, O24–O26, and O17–O18, O23–O25 distances for the sinusoidal ones (Fig. 1)]. Fig. 7 shows that the main diameters of [0 1 0] channel, very similar each other at P_{amb} (corresponding to an ellipticity (O1–O7)/(O5–O11) = 1), differentiate upon compression, reaching an ellipticity equal to 1.14 at 2 GPa. Between 0.3 and 1.2 GPa, a plateau is observed. The ellipticity of the channels running along [1 0 0] follows different zig-zag trends as a function of *P*, but, at 2 GPa, it assumes a value only slightly higher than the original one, conferring to the [1 0 0] channels a more circular shape with respect to the [0 1 0] one.

3.1.2. Extraframework sites

At P_{amb} 8 extraframework sites were located (Table 4) and labeled with the same symbols of the corresponding sites found in the natural analog mutinaite [28]. All these sites are completely or almost completely occupied at P_{amb}, providing a total electron number equal to 303, which is in excellent agreement with those derived from the chemical formula (307). From Table 4, one can see that some extra-framework sites are characterized by site occupancy factors (s.o.f.) higher that one. Considering a relative error equal to 3 times the standard deviations, the only s.o.f. significantly higher that one are those of X1 and X16 sites (1.20 and 1.17, respectively, in Table 4). However, these values can be justified by considering that H-ZSM-5 sample contains 1.1 Na atoms – modeled with the oxygen scattering curve – which, as a consequence, are expected to be distributed over these two sites.

The main effect of compression – occurring at $P \geq 0.8$ GPa – is the shift of some sites (X1, X15, X16) from their original positions with multiplicity = 4 to new ones with multiplicity = 8, as a consequence of the movement of X1 outside the inversion center and of X15 and X16 out of the mirror plane perpendicular to b axis (Table 4 and Figs. 5 and 6). In addition, starting from 0.8 GPa, two new extraframework sites (X14a and Xn) were located after the inspection of the the Fourier difference map. All these HP-induced changes in the extraframework system are completely reversible upon pressure release.

The P-induced re-organization of the extraframework system is accompanied by an increase of the total extraframework content, which can be ascribed to the penetration of extra molecules in the pores, which, due to the channel dimensions of H-ZSM-5, could be in principle both water and alcohol molecules. This phenomenon is clearly evidenced by Fig. 8, which shows an increase of the total electron number of the extraframework sites, in particular starting from 0.5 GPa. The additional medium molecules which penetrate H-ZSM-5 structure at 2.0 GPa (Table 4) are distributed over the two new sites X14a and Xn, and over other sites (X1, X5, X15 and X16), already present in the P_{amb} structure, but moved from their original position. This P-induced penetration effect produces an increase of about 34% of the extraframework total electron number, which is the highest up to now observed in zeolites which undergo this phenomenon without any cell volume expansion [12,15,16]. Notwithstanding this, due to the impossibility to perform complete

Table 4
Refined atomic positions and displacement parameters (Å^2) of H-ZSM-5 in m.e.w. at selected pressure values.

	P_{amb}					0.8 Gpa				
	x/*a*	*y*/*b*	*z*/*c*	Occ.	U_{iso}	*x*/*a*	*y*/*b*	*z*/*c*	Occ.	U_{iso}
Si1	0.423(2)	0.062(2)	−0.328(3)	1	0.019(2)	0.422(2)	0.065(2)	−0.334(2)	1	0.017(2)
Si2	0.309(2)	0.027(2)	−0.187(3)	1	0.019(2)	0.308(2)	0.029(1)	−0.192(2)	1	0.017(2)
Si3	0.280(2)	0.061(2)	0.031(3)	1	0.019(2)	0.276(2)	0.057(2)	0.025(2)	1	0.017(2)
Si4	0.124(2)	0.059(2)	0.035(2)	1	0.019(2)	0.116(2)	0.063(2)	0.030(2)	1	0.017(2)
Si5	0.073(2)	0.027(2)	−0.184(3)	1	0.019(2)	0.074(2)	0.030(2)	−0.191(2)	1	0.017(2)
Si6	0.186(2)	0.060(2)	−0.322(3)	1	0.019(2)	0.183(2)	0.057(2)	−0.333(2)	1	0.017(2)
Si7	0.423(2)	−0.170(1)	−0.320(3)	1	0.019(2)	0.421(2)	−0.169(1)	−0.322(3)	1	0.017(2)
Si8	0.308(2)	−0.133(2)	−0.172(3)	1	0.019(2)	0.300(2)	−0.130(1)	−0.191(2)	1	0.017(2)
Si9	0.273(2)	−0.177(2)	0.048(2)	1	0.019(2)	0.281(2)	−0.177(2)	0.031(2)	1	0.017(2)
Si10	0.113(2)	−0.175(2)	0.021(3)	1	0.019(2)	0.120(2)	−0.173(2)	0.022(2)	1	0.017(2)
Si11	0.063(2)	−0.135(2)	−0.196(3)	1	0.019(2)	0.066(2)	−0.131(2)	−0.194(2)	1	0.017(2)
Si12	0.191(3)	−0.174(1)	−0.322(2)	1	0.019(2)	0.184(2)	−0.180(1)	−0.341(2)	1	0.017(2)
O1	0.376(3)	0.064(4)	−0.230(4)	1	0.037(4)	0.372(3)	0.069(4)	−0.238(4)	1	0.059(4)
O2	0.315(3)	0.059(3)	−0.077(3)	1	0.037(4)	0.312(4)	0.063(2)	−0.082(3)	1	0.059(4)
O3	0.202(2)	0.064(4)	0.010(4)	1	0.037(4)	0.197(2)	0.060(4)	0.018(4)	1	0.059(4)
O4	0.097(3)	0.053(4)	−0.079(3)	1	0.037(4)	0.108(3)	0.050(4)	−0.088(3)	1	0.059(4)
O5	0.115(2)	0.067(3)	−0.267(5)	1	0.037(4)	0.112(2)	0.065(3)	−0.282(4)	1	0.059(4)
O6	0.245(3)	0.057(5)	−0.245(5)	1	0.037(4)	0.239(3)	0.042(5)	−0.254(5)	1	0.059(4)
O7	0.375(3)	−0.161(4)	−0.223(5)	1	0.037(4)	0.368(3)	−0.164(4)	−0.231(4)	1	0.059(4)
O8	0.305(3)	−0.149(3)	−0.057(3)	1	0.037(4)	0.307(3)	−0.155(3)	−0.081(3)	1	0.059(4)
O9	0.192(2)	−0.169(3)	0.038(4)	1	0.037(4)	0.200(2)	−0.165(3)	0.018(4)	1	0.059(4)
O10	0.086(4)	−0.153(4)	−0.086(3)	1	0.037(4)	0.092(3)	−0.144(4)	−0.084(3)	1	0.059(4)
O11	0.126(3)	−0.146(5)	−0.266(5)	1	0.037(4)	0.125(3)	−0.154(4)	−0.268(4)	1	0.059(4)
O12	0.249(3)	−0.150(4)	−0.249(5)	1	0.037(4)	0.242(3)	−0.159(4)	−0.265(5)	1	0.059(4)
O13	0.303(4)	−0.053(2)	−0.175(4)	1	0.037(4)	0.313(4)	−0.052(1)	−0.179(4)	1	0.059(4)
O14	0.069(4)	−0.055(2)	−0.198(4)	1	0.037(4)	0.069(4)	−0.052(2)	−0.206(4)	1	0.059(4)
O15	0.415(4)	0.134(3)	−0.384(4)	1	0.037(4)	0.424(3)	0.139(2)	−0.388(5)	1	0.059(4)
O16	0.399(4)	0.004(3)	−0.400(4)	1	0.037(4)	0.397(3)	0.004(2)	−0.403(4)	1	0.059(4)
O17	0.402(5)	−0.129(3)	−0.418(4)	1	0.037(4)	0.403(4)	−0.138(2)	−0.428(3)	1	0.059(4)
O18	0.180(3)	0.129(2)	−0.387(4)	1	0.037(4)	0.177(3)	0.128(2)	−0.395(4)	1	0.059(4)
O19	0.204(4)	−0.002(3)	−0.393(4)	1	0.037(4)	0.184(3)	0.000(2)	−0.418(4)	1	0.059(4)
O20	0.200(5)	−0.132(3)	−0.426(4)	1	0.037(4)	0.200(5)	−0.130(3)	−0.436(3)	1	0.059(4)
O21	0.001(2)	0.060(4)	−0.198(5)	1	0.037(4)	0.002(2)	0.067(4)	−0.183(5)	1	0.059(4)
O22	−0.010(2)	−0.154(4)	−0.240(4)	1	0.037(4)	−0.009(2)	−0.149(4)	−0.234(4)	1	0.059(4)
O23	0.420(7)	0.75	−0.340(9)	1	0.037(4)	0.415(5)	0.75	−0.335(9)	1	0.059(4)
O24	0.181(6)	0.75	−0.359(5)	1	0.037(4)	0.180(4)	0.75	−0.398(4)	1	0.059(4)
O25	0.303(5)	0.75	0.078(6)	1	0.037(4)	0.284(5)	0.75	0.088(5)	1	0.059(4)
O26	0.101(5)	0.75	0.062(7)	1	0.037(4)	0.108(5)	0.75	0.056(7)	1	0.059(4)
X1	0.5	0	0	1.20(5)	0.061(6)	0.507(2)	0.055(2)	0.043(4)	0.92(3)	0.069(6)
X5	0.039(2)	0.25	0.585(4)	0.82(5)	0.061(6)	0.020(3)	0.25	0.472(3)	1.10(6)	0.069(6)
X9	0.003(2)	0.149(2)	0.494(3)	1.08(4)	0.061(6)	0.983(2)	0.150(1)	0.568(3)	1.16(4)	0.069(6)
X11	0.392(3)	0.25	0.910(4)	0.97(5)	0.061(6)	0.403(3)	0.25	0.843(4)	1.00(5)	0.069(6)
X13	0.467(2)	0.25	0.765(4)	1.02(6)	0.061(6)	0.528(6)	0.25	0.843(8)	0.54(4)	0.069(6)
X14	0.089(3)	0.25	0.761(4)	1.11(6)	0.061(6)	0.034(7)	0.25	0.842(1)	0.58(9)	0.069(6)
X15	0.280(2)	0.25	0.831(4)	1.02(5)	0.061(6)	0.280(2)	0.25	0.815(4)	1.18(6)	0.069(6)
X16	0.139(2)	0.25	0.929(3)	1.17(4)	0.061(6)	0.151(3)	0.25	0.898(4)	1.06(4)	0.069(6)
X14a	–	–	–	–	–	0.059(5)	0.25	0.723(1)	0.59(9)	0.069(6)
Xn	–	–	–	–	–	–	–	–	–	–

	2.0 GPa					P_{amb} (rev)				
	x/a	*y/b*	*z/c*	Occ.	U_{iso}	*x/a*	*y/b*	*z/c*	Occ.	U_{iso}
Si1	0.428(1)	0.076(1)	−0.338(2)	1	0.026(2)	0.427(2)	0.062(2)	−0.320(2)	1	0.021(2)
Si2	0.303(1)	0.310(1)	−0.204(2)	1	0.026(2)	0.301(2)	0.027(1)	−0.191(3)	1	0.021(2)
Si3	0.284(1)	0.062(1)	0.017(2)	1	0.026(2)	0.286(1)	0.063(2)	0.031(2)	1	0.021(2)
Si4	0.122(1)	0.045(1)	0.018(2)	1	0.026(2)	0.128(1)	0.050(2)	0.030(2)	1	0.021(2)
Si5	0.068(1)	0.027(1)	−0.203(2)	1	0.026(2)	0.073(2)	0.034(1)	−0.179(2)	1	0.021(2)
Si6	0.174(1)	0.056(1)	−0.343(2)	1	0.026(2)	0.178(2)	0.061(2)	−0.333(2)	1	0.021(2)
Si7	0.412(2)	−0.171(1)	−0.355(2)	1	0.026(2)	0.424(2)	−0.168(1)	−0.335(2)	1	0.021(2)
Si8	0.305(1)	−0.132(1)	−0.192(2)	1	0.026(2)	0.308(2)	−0.133(1)	−0.187(2)	1	0.021(2)
Si9	0.275(1)	−0.172(1)	0.030(2)	1	0.026(2)	0.271(2)	−0.184(1)	0.027(2)	1	0.021(2)
Si10	0.115(1)	−0.180(1)	0.009(2)	1	0.026(2)	0.113(2)	−0.172(1)	0.033(2)	1	0.021(2)
Si11	0.059(1)	−0.135(1)	−0.203(2)	1	0.026(2)	0.070(2)	−0.128(1)	−0.187(2)	1	0.021(2)
Si12	0.186(2)	−0.175(1)	−0.337(2)	1	0.026(2)	0.188(2)	−0.177(1)	−0.322(2)	1	0.021(2)
O1	0.367(2)	0.067(1)	−0.258(3)	1	0.053(4)	0.374(3)	0.053(4)	−0.230(4)	1	0.054(4)
O2	0.306(3)	0.074(1)	−0.100(2)	1	0.053(4)	0.307(4)	0.065(3)	−0.085(3)	1	0.054(4)
O3	0.205(1)	0.049(4)	0.007(4)	1	0.053(4)	0.208(1)	0.048(4)	0.018(4)	1	0.054(4)
O4	0.099(3)	0.045(3)	−0.097(2)	1	0.053(4)	0.097(3)	0.066(3)	−0.079(3)	1	0.054(4)
O5	0.115(2)	0.075(2)	−0.270(3)	1	0.053(4)	0.111(2)	0.070(3)	−0.270(4)	1	0.054(4)
O6	0.238(2)	0.051(4)	−0.273(4)	1	0.053(4)	0.239(3)	0.051(4)	−0.261(4)	1	0.054(4)
O7	0.370(2)	−0.157(3)	−0.252(3)	1	0.053(4)	0.378(3)	−0.150(4)	−0.237(4)	1	0.054(4)
O8	0.309(3)	−0.161(2)	−0.083(2)	1	0.053(4)	0.298(4)	−0.148(3)	−0.075(3)	1	0.054(4)
O9	0.193(1)	−0.167(2)	0.030(4)	1	0.053(4)	0.192(2)	−0.166(3)	0.037(4)	1	0.054(4)
O10	0.091(3)	−0.157(3)	−0.100(3)	1	0.053(4)	0.092(3)	−0.144(3)	−0.076(3)	1	0.054(4)
O11	0.121(2)	−0.147(4)	−0.279(4)	1	0.053(4)	0.118(3)	−0.161(4)	−0.268(4)	1	0.054(4)
O12	0.243(1)	−0.160(4)	−0.257(3)	1	0.053(4)	0.239(3)	−0.152(4)	−0.240(4)	1	0.054(4)
O13	0.303(1)	−0.051(1)	−0.205(4)	1	0.053(4)	0.302(4)	−0.054(1)	−0.183(4)	1	0.054(4)
O14	0.07(3)	−0.056(2)	−0.215(4)	1	0.053(4)	0.076(3)	−0.048(1)	−0.194(4)	1	0.054(4)
O15	0.431(3)	0.146(2)	−0.404(4)	1	0.053(4)	0.425(4)	0.136(3)	−0.374(4)	1	0.054(4)
O16	0.401(3)	0.021(2)	−0.418(3)	1	0.053(4)	0.404(3)	−0.002(2)	−0.385(4)	1	0.054(4)
O17	0.395(3)	−0.123(2)	−0.448(4)	1	0.053(4)	0.395(4)	−0.123(3)	−0.426(4)	1	0.054(4)
O18	0.170(2)	0.128(2)	−0.407(4)	1	0.053(4)	0.195(4)	0.129(2)	−0.398(4)	1	0.054(4)
O19	0.173(2)	−0.002(2)	−0.432(3)	1	0.053(4)	0.181(3)	−0.002(2)	−0.408(4)	1	0.054(4)
O20	0.185(3)	−0.131(2)	−0.442(3)	1	0.053(4)	0.195(5)	−0.136(2)	−0.425(3)	1	0.054(4)
O21	0.001(2)	0.072(3)	−0.218(4)	1	0.053(4)	0.004(2)	0.065(4)	−0.216(4)	1	0.054(4)
O22	−0.022(3)	−0.146(3)	−0.208(4)	1	0.053(4)	−0.002(2)	−0.160(4)	−0.213(4)	1	0.054(4)
O23	0.403(4)	0.75	−0.388(5)	1	0.053(4)	0.421(6)	0.750	−0.348(7)	1	0.054(4)
O24	0.181(5)	0.75	−0.382(4)	1	0.053(4)	0.180(6)	0.750	−0.374(4)	1	0.054(4)
O25	0.276(4)	0.75	0.072(5)	1	0.053(4)	0.299(5)	0.750	0.083(5)	1	0.054(4)
O26	0.095(4)	−0.25	0.062(4)	1	0.053(4)	0.105(5)	0.750	0.062(7)	1	0.054(4)
X1	0.526(1)	0.054(1)	1.070(2)	1.22(6)	0.034(6)	0.500	0.000	0.000	0.99(5)	0.058(5)
X5	−0.003(1)	0.25	0.432(3)	1.13(6)	0.034(6)	0.057(5)	0.250	0.581(5)	0.54(5)	0.058(5)
X9	0.973(2)	0.150(2)	0.524(4)	0.77(6)	0.034(6)	0.011(2)	0.154(2)	0.486(3)	1.17(3)	0.058(5)
X11	0.392(2)	0.25	0.893(3)	1.05(6)	0.034(6)	0.386(2)	0.250	0.895(3)	1.09(5)	0.058(5)
X13	0.518(2)	0.25	0.883(3)	0.54(6)	0.034(6)	0.480(2)	0.250	0.775(5)	0.90(5)	0.058(5)
X14	0.094(3)	0.25	0.759(4)	1.03(6)	0.034(6)	0.097(2)	0.250	0.782(4)	1.05(6)	0.058(5)
X15	0.286(2)	0.215(3)	0.805(2)	0.71(6)	0.034(6)	0.260(3)	0.250	0.823(4)	0.99(5)	0.058(5)
X16	0.179(2)	0.187(3)	0.897(2)	1.06(6)	0.034(6)	0.163(3)	0.250	0.940(4)	0.90(4)	0.058(5)
X14a	0.484(4)	0.25	0.723(5)	0.66(6)	0.034(6)	–	–	–	–	–
Xn	0.062(3)	0.233(3)	0.571(4)	0.39(6)	0.034(6)	–	–	–	–	–

Table 5
T-O framework distances (Å) for H-ZSM-5 in m.e.w. at selected pressures.

	P_{amb}	0.8 GPa	2.0 GPa	P_{amb} (rev)
Si1 –				
O1	1.635(13)	1.631(15)	1.632(14)	1.632(16)
O15	1.633(13)	1.644(15)	1.642(14)	1.655(17)
O16	1.589(13)	1.605(15)	1.614(13)	1.614(16)
O21	1.608(13)	1.620(15)	1.625(14)	1.613(17)
Mean	*1.616*	*1.625*	*1.628*	*1.629*
Si2 –				
O1	1.636(13)	1.637(15)	1.625(14)	1.641(17)
O2	1.613(13)	1.616(15)	1.635(14)	1.620(16)
O6	1.623(13)	1.627(15)	1.625(13)	1.632(16)
O13	1.617(13)	1.619(15)	1.624(13)	1.618(16)
Mean	*1.622*	*1.625*	*1.628*	*1.628*
Si3 –				
O2	1.622(13)	1.605(15)	1.633(14)	1.631(16)
O3	1.593(13)	1.598(15)	1.608(13)	1.607(16)
O19	1.598(13)	1.592(15)	1.598(13)	1.621(16)
O20	1.589(13)	1.603(15)	1.596(14)	1.604(17)
Mean	*1.601*	*1.600*	*1.609*	*1.616*
Si4 –				
O3	1.623(13)	1.632(15)	1.640(13)	1.633(15)
O4	1.624(13)	1.616(15)	1.609(14)	1.615(16)
O16	1.604(13)	1.622(15)	1.624(13)	1.629(16)
O17	1.635(13)	1.641(15)	1.641(14)	1.638(17)
Mean	*1.622*	*1.628*	*1.629*	*1.629*
Si5 –				
O4	1.583(13)	1.583(15)	1.583(14)	1.570(16)
O5	1.614(13)	1.601(15)	1.599(14)	1.601(17)
O14	1.653(13)	1.647(15)	1.650(13)	1.653(16)
O21	1.605(13)	1.622(15)	1.604(14)	1.611(17)
Mean	*1.614*	*1.613*	*1.609*	*1.609*
Si6 –				
O5	1.603(13)	1.590(15)	1.606(14)	1.595(17)
O6	1.586(13)	1.581(15)	1.596(13)	1.582(16)
O18	1.636(13)	1.635(15)	1.643(14)	1.655(16)
O19	1.611(13)	1.615(15)	1.625(14)	1.615(16)
Mean	*1.609*	*1.605*	*1.618*	*1.612*
Si7 –				
O7	1.634(13)	1.628(15)	1.621(14)	1.642(16)
O17	1.598(13)	1.596(15)	1.592(14)	1.627(17)
O22	1.622(13)	1.640(15)	1.623(14)	1.639(17)
O23	1.620(13)	1.632(15)	1.642(13)	1.655(15)
Mean	*1.619*	*1.624*	*1.620*	*1641*
Si8 –				
O7	1.601(13)	1.602(15)	1.596(14)	1.598(17)
O8	1.583(13)	1.573(15)	1.573(14)	1.560(16)
O12	1.620(13)	1.620(15)	1.609(14)	1.618(16)
O13	1.597(13)	1.599(15)	1.599(13)	1.599(16)
Mean	*1.616*	*1.599*	*1.594*	*1.594*
Si9 –				
O8	1.658(13)	1.662(15)	1.656(14)	1.638(16)
O9	1.646(13)	1.650(15)	1.625(13)	1.635(16)
O18	1.608(13)	1.630(15)	1.608(14)	1.636(16)
O25	1.622(13)	1.632(15)	1.646(13)	1.616(17)
Mean	*1.634*	*1.644*	*1.634*	*1.631*
Si10 –				
O9	1.614(13)	1.619(15)	1.599(13)	1.603(16)
O10	1.607(13)	1.622(15)	1.598(13)	1.623(16)
O15	1.616(13)	1.636(15)	1.623(14)	1.635(17)
O26	1.617(13)	1.623(15)	1.608(14)	1.624(15)
Mean	*1.614*	*1.625*	*1.607*	*1.621*
Si11 –				
O10	1.589(13)	1.587(15)	1.568(13)	1.595(16)
O11	1.608(13)	1.622(15)	1.611(14)	1.604(17)
O14	1.606(13)	1.592(15)	1.594(14)	1.609(16)
O22	1.620(13)	1.630(15)	1.612(14)	1.626(17)
Mean	*1.606*	*1.608*	*1.596*	*1.609*
Si12 –				
O11	1.603(13)	1.614(15)	1.605(14)	1.609(17)
O12	1.596(13)	1.591(15)	1.587(14)	1.585(16)
O20	1.635(13)	1.654(15)	1.652(14)	1.623(16)
O24	1.619(13)	1.601(15)	1.594(14)	1.618(16)
Mean	*1.613*	*1.615*	*1.610*	*1.609*

Table 6
Interatomic distances (< 3.20 Å) of the extraframework sites for selected refinements of H-ZSM-5 compressed in m.e.w.

	P_{amb}		0.8 GPa		2.0 GPa		P_{amb} (rev)	
X1-								
X1			2.48(7)		3.02(5)			
X9	2.97(3)	X2	2.46(4)		2.50(2)		3.08(3)	X2
X5-								
O25	3.19(7)						2.89(1)	
X9	2.48(9)	X2	2.48(7)	X2	2.38(5)	X2	2.49(1)	X2
X11	2.97(9)							
X13	2.49(7)		2.49(1)		2.50(2)		2.49(9)	
X14	2.56(7)						2.83(7)	
X14a					2.27(7)	X2		
X9-								
X1	2.97(3)		2.46(4)		2.50(4)		3.08(3)	
X5	2.48(9)		2.48(7)		2.38(4)		2.49(1)	
X11			2.82(6)		2.78(4)			
X13			2.48(8)		2.50(4)			
X14a					2.49(2)			
X11-								
X5	2.97(9)							
X9			2.82(6)	X2	2.78(4)	X2		
X13	2.48(1)		2.49(2)		2.50(2)		2.49(2)	
X14a								
X15	2.49(1)		2.50(1)		2.50(2)	X2	2.72(6)	
Xn					2.91(6)			
X13-								
O26	3.04(6)							
X5	2.49(7)		2.49(1)		2.50(2)		2.49(9)	
X9			2.48(8)	X2	2.50(4)	X2		
X11	2.48(1)		2.49(2)		2.50(2)		2.49(2)	
X14	2.49(6)		2.49(2)		2.33(6)		2.48(2)	
X14a			1.08(2)		1.12(8)	X2		
Xn					2.24(8)			
X14-								
O15			3.17(5)	X2				
O26			3.16(9)					
X5	2.56(7)						2.83(7)	
X13	2.49(6)		2.49(2)		2.33(6)		2.49(2)	
X14a			1.67(2)		2.50(6)	X2		
X16	2.49(7)		2.48(2)		2.86(4)	X2	2.49(2)	
Xn					2.21(7)			
X15-								
X11	2.49(1)		2.50(1)		2.50(2)		2.72(6)	
X15					1.19(1)			
X16	3.14(7)		2.79(9)		2.51(4)		2.52(8)	
X16-								
O3					3.15(2)			
O17					2.85(2)			
X14	2.49(7)		2.48(2)		2.86(5)		2.49(2)	
X14a			3.00(2)					
X15	3.14(7)		2.79(9)		2.51(4)		2.52(8)	
X15					3.03(5)			
X16					2.47(2)			
X14*a*								
O18					3.00(5)			
X5					2.27(2)			
X9					2.49(2)			
X13			1.08(2)		1.12(8)			
X14			1.67(2)		2.50(2)			
X16			3.00(2)					
X14a					0.6(2)			
Xn–								
O15					2.83(5)	X2		
O26					2.53(6)			
X11					2.68(8)			
X13					2.24(8)			
X14					2.21(8)			

structure refinements of the patterns collected at higher *P*, we cannot exclude that even further medium molecules penetrate the structure above 2.0 GPa.

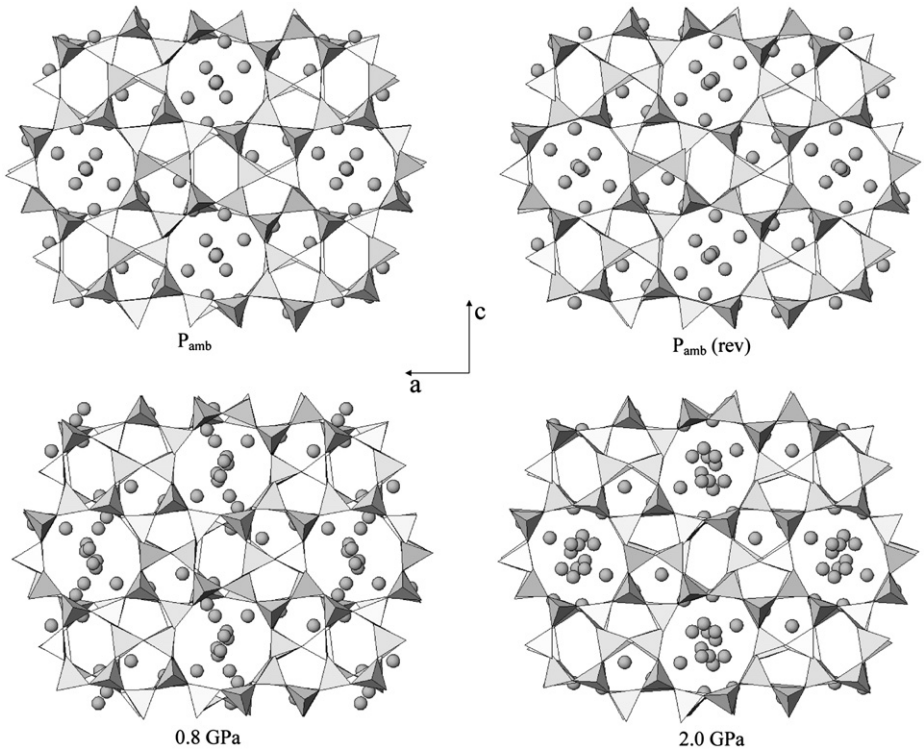

Fig. 5. Projection of the H-ZSM-5 structure along the [0 1 0] direction at P_{amb}, 0.8, 2.0 GPa and P_{amb} (rev).

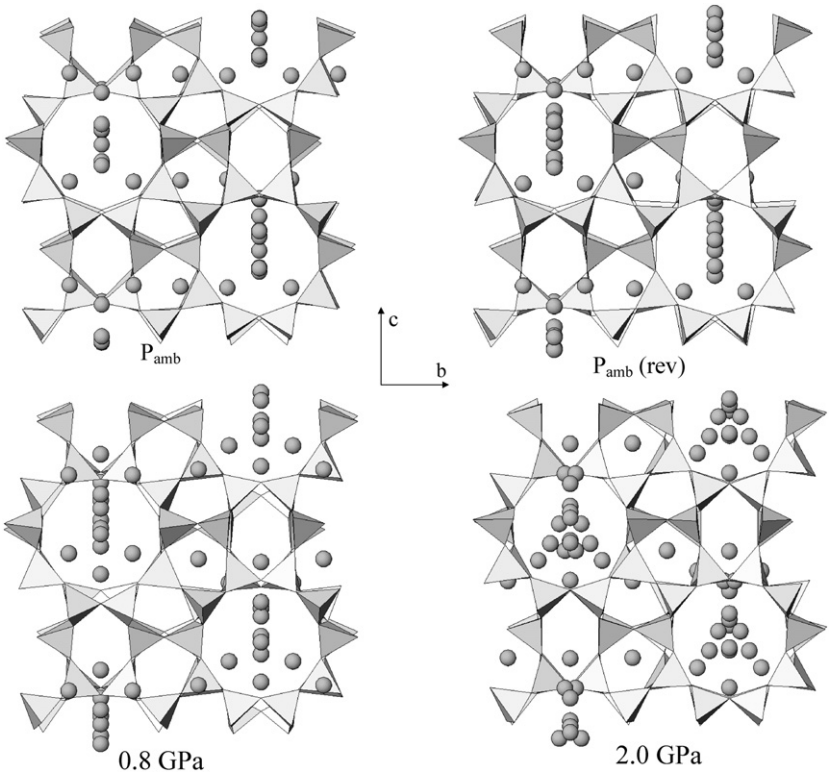

Fig. 6. Projection of the H-ZSM-5 structure along the [1 0 0] direction at P_{amb}, 0.8, 2.0 GPa and P_{amb} (rev).

Table 6 shows that some X–X bond distances are too short, but acceptable on the basis of the sum of the occupancy factors of the involved sites, which are hence mutually exclusive. Moreover, Table 6 shows that, at 2 GPa, three of the sites which host the new extra molecules (X16, X14a, and Xn) become bonded to framework oxygen atoms belonging to the [1 0 0] channel apertures (O15, O17, O18, and O26 in Fig. 1). These interactions contribute to stiffen the structure and could be at the origin of the lower decrease of the unit cell volume of H-ZSM-5 compressed in m.e.w. with respect to s.o.

Table 7
Diagonal O…O distances (Å) and ellipticity of the straight and sinusoidal 10-ring channels of H-ZSM-5 in the pressure range P_{amb}–2.0 GPa.

P (GPa)	Straight channel along [0 1 0]		
	O5–O11	O1–O7	(O1–O7)/(O5–O11)
P_{amb}	8.11(1)	8.14(1)	1.00
0.1	7.99	8.18	1.02
0.3	7.93	8.40	1.06
0.5	7.95	8.35	1.05
0.8	7.87	8.38	1.06
1.2	8.36	8.62	1.03
1.6	7.59	8.84	1.16
2.0	7.74	8.80	1.14
P_{amb} (rev)	7.97	8.27	1.04

P (GPa)	Sinusoidal channels along [1 0 0]					
	O15–O20	O24–O26	O23–O25	O17–O18	O15–O20/O24–O26	O17–O18/O23–O25
P_{amb}	8.07(1)	7.95(1)	8.18(1)	8.12(1)	1.02	0.99
0.1	8.02	7.82	8.02	8.23	1.03	1.03
0.3	8.07	7.53	8.25	8.11	1.07	0.98
0.5	7.98	7.66	8.00	7.90	1.04	0.99
0.8	8.00	7.46	8.17	7.97	1.07	0.98
1.2	8.07	7.68	7.51	7.79	1.05	1.04
1.6	8.10	7.61	7.83	8.25	1.06	1.05
2.0	7.92	7.60	7.63	7.95	1.04	1.04
P_{amb} (rev)	7.96	7.74	8.04	8.26	1.03	1.03

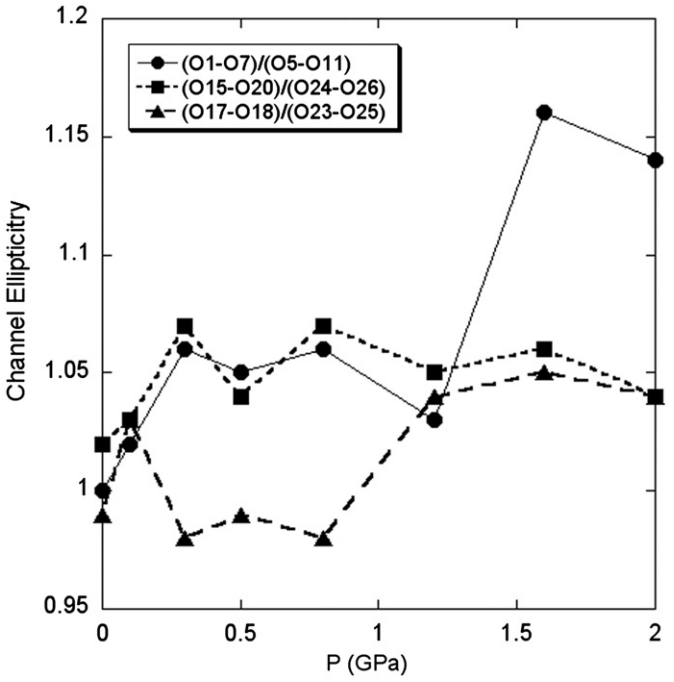

Fig. 7. Pressure-dependence of the window ellipticity of the 10-ring straight channel running along [0 1 0] and of the two 10-ring sinusoidal channels running along [1 0 0]. The errors associated with the data are of the same order of magnitude of their errors. Atoms labels are the same of Fig. 1.

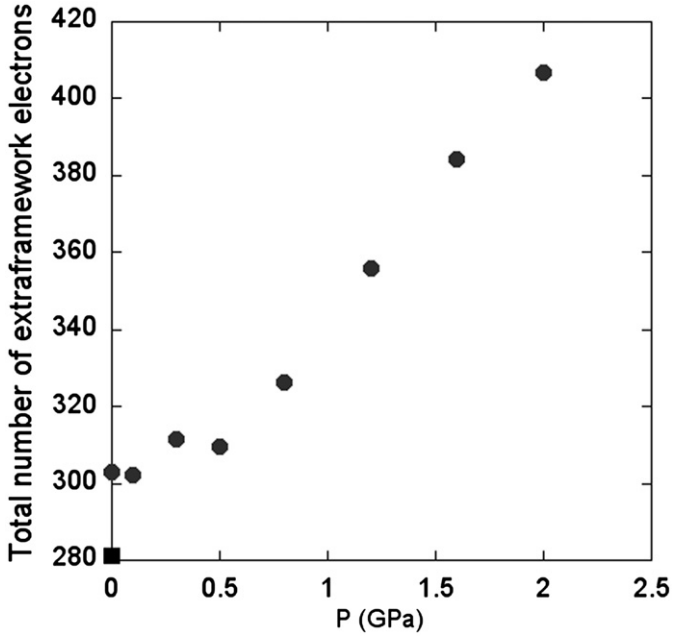

Fig. 8. P-dependence of the electron numbers of the extraframework sites of H-ZSM-5 compressed in m.e.w. Black square represents the number of extraframework electrons at P_{amb} after decompression.

3.2. Comparative discussion of H-ZSM-5 elastic behavior

The comparison between the deformations undergone by H-ZSM-5 in m.e.w. and in s.o. can be done between P_{amb} and 6.2 GPa. In this *P* range, the unit cell volume reduction in m.e.w. (about 12%) is significantly lower than that observed in s.o. (16.6%) (Fig. 9), indicating a more "rigid" behavior of this microporous material when compressed in the aqueous medium. A similar behavior has been recently observed by our group in boggsite [15] and Na-ZSM-5 [16], and has been interpreted as due to the penetration of additional water/alcohol molecules in the pores, which contrast the HP-induced structural deformation. Silicone oil molecules cannot penetrate, therefore all pressure exerted on the sample goes directly into compression of the framework and leads to a higher compressibility. The main difference in the two *P*/*V* curve slopes of Fig. 9 is observed at low pressure – where medium penetration is demonstrated to occur – while, above 3 GPa, they become almost parallel, suggesting a similar deformation mechanism.

The elastic parameters of H-ZSM-5 in s.o, obtained using a second order Birch–Murnaghan equation of state and data

weighted by the uncertainties in P and V, are $V_0=5473(9)$ Å^3, $K_0=23.7(4)$ GPa. The refined linear axial bulk moduli are: K_0(a)=22.4(4); K_0(b)=20.1(3); K_0(c)=21.5(3) for the a, b, and c-axis, respectively. Since the bulk modulus values determined for zeolites compressed in "non-penetrating" media range from about 18 to 72 GPa [14], H-ZSM-5 can be classified as one of the most compressible zeolite up to now studied under these conditions.

The elastic parameters of H-ZSM-5 compressed in m.e.w. were calculated between 3.0 and 7.6 GPa, that is in the P range where the compressibility behavior is similar to that observed in s.o. (Fig. 9), hence, where we can assume that the medium penetration is finished. The bulk modulus, obtained using a truncated second-order Birch–Murnaghan equation of state and the data weighted by the uncertainties in P and V, was $K_0=27.4$ (6) GPa. The refined linear axial bulk modula are: K_0(a)=20.1(5); K_0(b)=32.0(9); K_0(c)=32.2(8) for the a, b, and c-axis, respectively. Notwithstanding the compressibility determined in m.e.w. is lower than that in s.o., it is one of the highest when compared with other natural and synthetic zeolites studied with "penetrating" aqueous media [12,15,16].

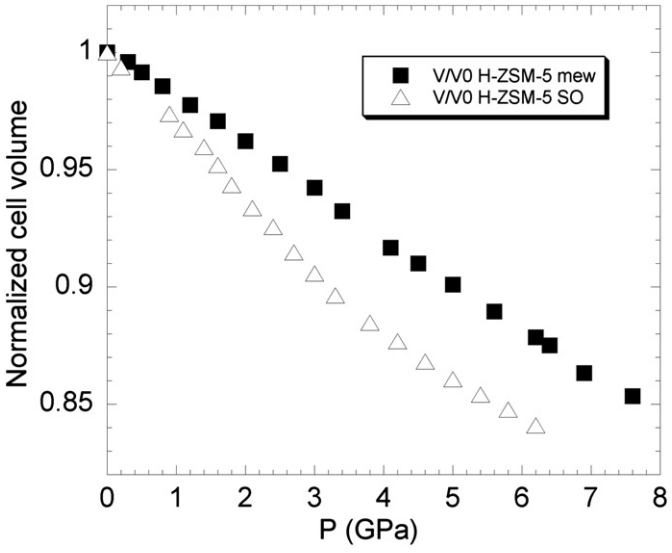

Fig. 9. Comparison of the unit-cell volume variations as a function of pressure for H-ZSM-5 compressed in silicone oil (triangles) and (16:3:1) methanol: ethanol:water (squares).

It is especially interesting to compare the HP behavior of H-ZSM-5 with that of Na-ZSM-5, the other zeolite with MFI topology recently studied by our group [16]. In s.o. (Fig. 10a) Na-ZSM-5 is more compressible ($K_0=18.2(2)$ GPa) than H-ZSM-5 ($K_0=23.7(4)$ GPa). This can be ascribed to the different extraframework water content (28 and 36 molecules in Na-ZSM-5 and H-ZSM-5, respectively), which allows a higher deformation in Na-ZSM-5. These findings suggest that the compressibility of MFI porous materials increases with increasing their hydrophobic character, that is their Si/Al ratio (20.4 and 11.4 for Na-ZSM-5 and H-ZSM-5, respectively). This conclusion is confirmed by the preliminary data obtained on two silicalite samples and on natural mutinaite, characterized by different Si/Al ratio and water content [17,18].

The compressibility in m.e.w. is, otherwise, very similar for the two phases (Fig. 10b), the bulk modulus values calculated after m.e.w. molecules penetration being $K_0=27.4$ (6) and 28.9 (5) GPa for H-ZSM-5 and Na-ZSM-5, respectively. The interpretation of this trend, however, is hindered by the lack of information on the actual total amount of extra medium molecules which penetrate the two phases. In fact, the structure refinements were performed only up to 2.0 and 1.6 GPa for H- and Na-ZSM-5, respectively.

It is worth noting that the increase of the extra-framework content of both H-ZSM-5 and Na-ZSM-5, although extremely high, occurs without any cell volume expansion, similarly to that found for gismondine [12], boggsite [15] and NaA [34], and contrary to that reported for other zeolites of the fibrous family [35–38]. The abrupt volume expansion observed in these last cases was ascribed to the penetration of additional water molecules in new extraframework sites, while in gismondine, boggsite and Na-ZSM-5 the extra molecules contribute to increase the occupancy of already existing extraframework sites. The case of H-ZSM-5 is different: here the penetrating molecules occupy both new and already existing sites, but, due to the larger dimensions of the channels with respect to fibrous zeolites, additional extra-framework positions can arise without volume expansion. As a confirm of this interpretation, one can claim the effects of pressure-induced over-hydration of zeolite Y and LTL: in these phases, the large 12-ring channels allows the penetration of extra water molecules without volume increase [39,40].

An interesting difference between H-ZSM-5 and Na-ZSM-5 concerns the reversibility of m.e.w. penetration: while the extra molecules are completely released upon decompression in H-ZSM-5, in Na-ZSM-5 the phenomenon is only partially reversible [16], and hence a material with a different extraframework composition is obtained at the end of the process.

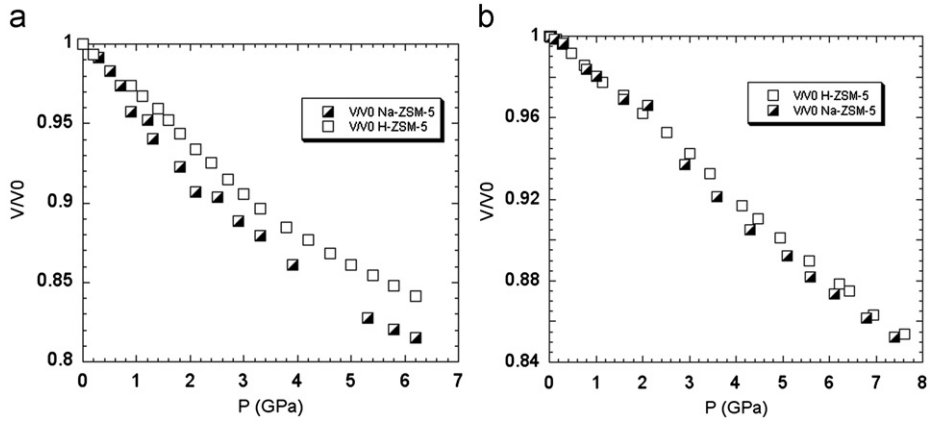

Fig. 10. Comparison between the elastic behavior of H-ZSM-5 and Na-ZSM-5 compressed in (a) silicone oil and (b) methanol:ethanol:water.

Acknowledgments

BM01 and ID09 beamlines at European Synchrotron Radiation Facility are acknowledged for allocation of the experimental beamtime. The authors are indebted with Vladimir Dmitriev and Marco Merlini for the assistance during the diffraction experiments. Simona Bigi is acknowledged for the chemical analysis of the samples. The authors thank an anonymous reviewer for the useful comments, which improved the manuscript.

References

[1] Baerlocher, W.M. Meier, D.H. Olson, Atlas of Zeolite Framework Types, Elsevier, The Netherlands, 2001.
[2] G.T. Kokotailo, S.L. Lawton, O.H. Olson, W.M. Meier, Nature 272 (1978) 437–438.
[3] D.H. Olson, G.T. Kokotailo, S.L. Lawton, W.M. Meier, J. Phys. Chem. 85 (1981) 2238–2243.
[4] D.G. Hay, H. Jaeger, J. Chem. Soc., Chem. Commun. (1984) 1433.
[5] E. de Vos Burchart, H. van Bekkum, B. van de Graaf, Zeolites 13 (1993) 212–215.
[6] H. van Koningsveld, J.C. Jansen, H. van Bekkum, Zeolites 7 (1987) 564–568.
[7] R. Arletti, O. Ferro, S. Quartieri, A. Sani, G. Tabacchi, G. Vezzalini, Am. Miner. 88 (2003) 1416–1422.
[8] E. Fois, A. Gamba, G. Tabacchi, R. Arletti, S. Quartieri, G. Vezzalini, Am. Miner. 90 (2005) 28–35.
[9] E. Fois, A. Gamba, G. Tabacchi, S. Quartieri, R. Arletti, G. Vezzalini, in: A. Gamba, C. Colella, S. Coluccia (Eds.), Oxide Based Materials, Studies in Surface Science and Catalysis Series, vol. 155, Elsevier Science B.V, Amsterdam, 2005, pp. 271–280.
[10] C. Betti, E. Fois, E. Mazzucato, C. Medici, S. Quartieri, G. Tabacchi, G. Vezzalini, V. Dmitriev, Micropor. Mesopor. Mater. 103 (2007) 190–209.
[11] S. Ori, S. Quartieri, G. Vezzalini, V. Dmitriev, Am. Miner. 93 (2008) 53–62.
[12] S. Ori, S. Quartieri, G. Vezzalini, V. Dmitriev, Am. Miner. 93 (2008) 1393–1403.
[13] E. Fois, A. Gamba, C. Medici, G. Tabacchi, S. Quartieri, E. Mazzucato, R. Arletti, G. Vezzalini, V. Dmitriev, Micropor. Mesopor. Mater. 115 (2008) 267–280.
[14] L. Leardini, S. Quartieri, G. Vezzalini, Micropor. Mesopor. Mater. 127 (2010) 219–227.
[15] R. Arletti, S. Quartieri, G. Vezzalini, Am. Mineral. 95 (2010) 1247–1256.
[16] R. Arletti, G. Vezzalini, A. Morsli, F. Di Renzo, V. Dmitriev, S. Quartieri, Micropor. Mesopor. Mater. 142 (2011) 696–707.
[17] S. Quartieri, G. Montagna, R. Arletti, G. Vezzalini, 2010, Meeting of the International Mineralogical Association, Budapest, August 2010.
[18] G. Montagna, G. Vezzalini, S. Quartieri, R. Arletti, F. Di Renzo (2010) International Zeolite Conference IZC2010, Sorrento, July 2010.
[19] M. Colligan, Y. Lee, T. Vogt, A.J. Celestian, J.B. Parise, W.G. Marshall, J.A. Hriljac, J. Phys. Chem. B. Lett. 109 (2005) 18223–18225.
[20] J.J. Donovan, M.L. Rivers in: J. R. Michael and P. Ingram (Eds.), Microbeam analysis, San Francisco 1990, pp. 66–68.
[21] R. Miletich, D.R. Allan, W.F. Kush, in: R.M. Hazen, R.T. Downs (Eds.), High-Temperature and High-Pressure Crystal Chemistry. Reviews in Mineralogy and Geochemistry, vol. 41, Washington, USA, 2000, pp. 445–519.
[22] R.A. Forman, G.J. Piermarini, J.D. Barnett, S. Block, Science 176 (1972) 284–285.
[23] H.K. Mao, J. Xu, P.M. Bell, J. Geophys. Res. 91 (1986) 4673–4676.
[24] A.P. Hammersley, S.O. Svensson, M. Hanfland, A.N. Fitch, D. Häusermann, High Pressure Res. 14 (1996) 235–248.
[25] A.C. Larson, R.B. Von Dreele, GSAS-General Structure Analysis System. Report LAUR 86–748, Los Alamos National Laboratory, Los Alamos, New Mexico, 1996.
[26] B.H. Toby, J. Appl. Crystallogr. 34 (2001) 210–213.
[27] P. Thomson, D.E. Cox, J.B. Hastings, J. Appl. Crystallogr. 20 (1987) 79–83.
[28] G. Vezzalini, S. Quartieri, E. Galli, A. Alberti, G. Cruciani, Å. Kvick, Zeolites 19 (1997) 323–325.
[29] X. Li, C. Gu, B. Zhong, Fenzi Cuihua 6 (1992) 104–111.
[30] R.J. Angel, EOS-FIT V6.0. Computer Program, Crystallography Laboratory, Department of Geological Sciences, Virginia Tech, Blacksburg, USA, 2001.
[31] F. Birch, Phys. Rev. 71 (1947) 809–824.
[32] R.J. Angel, in: R.M. Hazen, R.T. Downs (Eds.), High-Temperature and High-Pressure Crystal Chemistry, Rev. Mineral. and Geochem., vol. 41, 2000, pp. 35–59.
[33] H. van Koningsveld, J.C. Jansen, Micropor. Mesopor. Mater. 6 (1996) 159–167.
[34] A.Yu. Likhacheva, M.E. Malyshev, A. Manakov, S.V. Goryainov, A.I. Ancharov, Anomalous compression of scolecite and thomsonite in aqueous medium to 2 GPa, High Pressure Res. 26 (2006) 449–453.
[35] Lee, T. Vogt, J.A. Hriljac, J.B. Parise, G. Artioli, Pressure-induced volume expansion of zeolites in the natrolite family, J. Am. Chem. Soc. 124 (2002) 5466–5475.
[36] Yu.V. Seryotkin, V.V. Bakakin, B.A. Fursenko, I.A. Belitsky, W. Joswig, P.G. Radaelli, Structural evolution of natrolite during over-hydration: a high-pressure neutron diffraction study, Eur. J. Miner. 17 (2005) 305–313.
[37] A.Yu. Likhacheva, Y.V. Seryotkin, A. Manakov, S.V. Goryainov, A.I. Ancharov, Non-hydrostatic compression of zeolite NaA in water medium: connection to anomalous conductivity, Z. Kristallogr. 224 (1) (2006) 37–143.
[38] A.Yu. Likhacheva, Y.V. Seryotkin, A. Manakov, S.V. Goryainov, A.I. Ancharov, M.A. Sheromov, Pressure-induced over-hydration of thomsonite: a synchrotron powder diffraction study, Am. Miner. 92 (2007) 1610–1615.
[39] M. Colligan, P.M. Foster, A.K. Cheetman, Y. Lee, T. Vogt, J.A. Hriljac, Synchrotron X-ray powder diffraction and computational investigation of purely siliceus zeolite Yunder pressure, J. Am. Chem. Soc. 126 (2004) 12015–12022.
[40] Yongjae Lee, Chi-Chang Kao, Sun Jin Kim, § Hyun-Hwi Lee, Dong Ryeol Lee, Tae Joo Shin, Jae-Young Choi, Chem. Mater. 19 (2007) 6252–6257.